Journal of Energy Chemistry 104 (2025) 312–323

Contents lists available at ScienceDirect

Journal of Energy Chemistry

journal homepage: www.elsevier.com/locate/jechem

http://www.journals.elsevier.com/journal-of-energy-chemistry/

Post-plasma carbon bed design for CO_2 conversion: Does size and insulation matter?

Colin O'Modhrain *, Yury Gorbanev, Annemie Bogaerts

Research Group PLASMANT, Department of Chemistry, University of Antwerp, Universiteitsplein 1 2610 Wilrijk, Belgium

ARTICLE INFO

Article history:
Received 30 October 2024
Revised 29 December 2024
Accepted 30 December 2024
Available online 18 January 2025

Keywords:
Carbon bed
Reverse Boudouard reaction
Warm plasma
CO_2 conversion

ABSTRACT

We present the performance of a post-plasma carbon bed for improving plasma-based CO_2 conversion, studying the effect of bed length and additional thermal bed insulation. The experiments were conducted using an atmospheric pressure gliding arc plasmatron in both high and low specific energy input (SEI) regimes. Each bed was equipped with a silo to enable continuous carbon feeding and operation for an order of 1 h, thus overcoming previous limitations in literature. Importantly, we derive an improved energy efficiency (EE) calculation with an accurate and unambiguous consideration of the key reaction contributions of both plasma and carbon bed. This derivation serves to highlight the inconsistencies that arise in determining EE in such a complex chemical system. We therefore advise and advocate for the use of energy cost (EC) as the key reported energy metric in systems using post-plasma carbon beds. The optimum conversion and energy metrics were obtained with the longest bed, reaching a conversion of 41%, an EE of 51% and an EC of 0.41 MJ/mol at high SEI. The design of the insulated bed and silo allow for previously unreported preheating of the carbon, which reduces oscillations observed in the conversion profiles of the short and long beds. Preheating of the external silo for the long bed also yields a near-complete removal of oscillations. Finally, when comparing our performance with results from literature for post-plasma carbon beds, our system clearly improves upon the state-of-the-art, both in absolute values of conversion and energy metrics at the same SEI, as well as by sustaining this improvement for extended periods of time.

1. Introduction

Carbon capture and utilisation (CCU) is growing in importance to mitigate anthropogenic emission of carbon dioxide (CO_2) into the atmosphere. Utilisation methods aim to convert the captured CO_2 into more useful chemical building blocks such as carbon monoxide (CO). Competing technologies under investigation in the field include thermocatalysis [1,2], electrocatalysis [3,4], photocatalysis [5,6] and plasma [7–9]. Plasma-based solutions offer a flexible option, which can quickly be switched on/off, compatible with a variable renewable energy supply and typically with a relatively small footprint. Different types of plasma have been investigated in this regard, with varying degrees of non-equilibrium between gas and electron temperatures [8]. Cold plasma devices such as dielectric barrier discharges (DBDs) exhibit a high degree of said non-equilibrium, with gas temperatures close to ambient and electron temperatures around two orders of magnitude greater. Such devices typically result in relatively high conversion (up to 40%), albeit at low energy efficiency (EE) (at maximum ca. 10%) [8,9]. Quasi-thermal, or "warm", plasma reactors have also been studied extensively, wherein the degree of non-equilibrium is much lower, and the gas temperature is often in the order of several thousand Kelvin. These setups are typically limited by the fraction of gas treated by the plasma and the rapid recombination of CO and O/O_2 into CO_2, resulting in lower conversions (10%–12%) but higher EE (30%–40%) than cold plasma discharges [8–10]. Basic reactor modifications (e.g. internal flow pattern variations [10]/electrode geometry [11]) fail to breach the EE target of 60% cited as the goal for plasma-based CO_2 conversion technology [7,8].

As mentioned above, the main factor hindering the process development is the recombination reaction of CO with O and/or O_2 (both formed from CO_2 plasmolysis) back into CO_2. Several post-plasma modifications have been investigated as directions

* Corresponding author.
E-mail address: colin.omodhrain@uantwerpen.be (C. O'Modhrain).

https://doi.org/10.1016/j.jechem.2024.12.066

to tackle this problem. Converging nozzles that constrict the post-discharge gas stream have shown promise when applied to warm plasmas [12,13]. Hecimovic et al. showed that a post-plasma nozzle improved the mixing of the cold insulating swirling gas with the high temperature gas from the discharge region, effectively quenching the gas temperature and reducing the recombination reaction [12]. Their nozzle was also water-cooled, allowing for further conductive heat dissipation through the walls. In their most recent work with an atmospheric pressure microwave (MW) plasma and a multi-channel water-cooled nozzle [14], they achieved a near five-fold conversion improvement (from 12% to 57%) at a specific energy input (SEI) of 7 eV/molecule. A clear disadvantage of water-cooled nozzles is the conductive heat-loss to the water-cooled nozzle walls, which requires heat-recovery systems to reduce the energy loss from the system. Furthermore, as the nozzle does not remove the O_2 produced, the addition of a nozzle does not inherently solve the problem that plasma-based CO_2 conversion results in a three-component mixture (CO_2/CO/O_2), which will result in further separation costs downstream in an industrialised setting.

Another promising direction for enhancing CO_2 conversion performance in warm plasmas is the removal of the formed O_2 via absorbing membranes inserted into the effluent stream. Antunes et al. recently demonstrated this proof of concept using perovskite membranes downstream in an atmospheric pressure MW discharge [15]. Under their best conditions, they managed to remove ca. 5% of the produced O_2 from the effluent stream. The technology shows potential but is currently operated with an inert gas (argon in this study), which will incur further costs upon scaling up.

An alternative post-plasma modification with the same goal of removing O_2 from the effluent is the implementation of a carbon bed, wherein a solid carbonaceous material is added into a reaction chamber close to the discharge. This material, often derived from other waste streams [16,17], can react with the effluent species, potentially boosting conversion while simultaneously removing O_2 and increasing the output concentration of the desired product CO (see Eqs. (1)–(3)). The main reactions between gaseous species and solid carbon involved in this process are [18]:

$$O + C \rightleftharpoons CO \quad (1)$$

$$O_2 + 2C \rightleftharpoons 2CO \quad (2)$$

$$CO_2 + C \rightleftharpoons 2CO \quad (3)$$

with the addition of reactants such as solid carbon to a system, the inherent complexity increases and several reactions may proceed concurrently, such as CO_2 dissociation and the reverse Boudouard reaction (RBR, Eq. (3)).

To the best of our knowledge, there are no publications to date which collate all current works on the topic. Hence, in Section 2 we first present a detailed overview of current works on this topic. After describing the experimental setup (Section 3), we then derive more accurate equations for the calculation of EE, including the relative pertinent reaction contributions and their assumptions, in Section 4. Therein, we also highlight the fact that the calculation of EC is more straightforward and requires fewer assumptions. In Section 5, we present our results and discuss in detail the varied performances of the three carbon bed designs. Additionally, we collate the literature works with their best performance metrics (CO_2 conversion, EE and energy cost (EC)) summarized, together with our best results in this section.

2. Literature overview of plasma-based CO_2 conversion with a post-plasma carbon bed

One of the first reported cases of such a method applied to a plasma system was by Uhm et al. [19], wherein the authors introduced a coal powder downstream from their CO_2 MW discharge. In this work, they initially characterised the effluent of the CO_2 discharge in the absence of the coal powders using optical emission spectroscopy (OES) to determine the rotational temperature (T_r) of hydroxyl radicals obtained from the dissociation of a miniscule fraction of H_2O molecules added to the inlet stream (1 vol%). This rotational temperature was assumed to be equal to the heavy particle temperature (T_g) due to fast rotational-translational relaxation that occurs at atmospheric pressure. The gas temperature ranged from 6700 K closest to the discharge decreasing to 2550 K at 9 cm downstream. When introducing the coal powders, they achieved an optimum conversion of 40% at their highest SEI condition (24 kJ/L, 5.99 eV/molecule, i.e., high power of 4 kW and low flow rate of 10 L/min).

Liu et al. [20] utilised an atmospheric pressure thermal plasma torch operated in Ar and CO_2 to react with coke particles of 5–8 mm in diameter. In terms of conversion, their best result (95% conversion) was obtained using an applied power of 16 kW to a discharge composed of a near 1:1 mixture of Ar and CO_2 (25 and 26 L/min, respectively). Increasing the CO_2 fraction to a maximum of 1:1.4 (Ar:CO_2) at a fixed applied power (14 kW) resulted in a lower conversion of 68%, albeit with an improved EE of 82% and EC of 0.34 MJ/mol CO. It should be noted that this EE value is most likely slightly overestimated due to the competing reactions of pure CO_2 dissociation and the reverse Boudouard reaction (RBR), with the latter having a lower standard reaction enthalpy. As mentioned in Section 1, the over- or underestimation of EE is commonplace in post-plasma carbon bed literature due to these competing reactions. Therefore, we outline a new calculation in this work to account for this, as given in Section 4 (Metrics calculation and analysis).

Li et al. [21] followed up the work on this setup, investigating the influence of injecting the CO_2 into the afterglow of the thermal plasma discharge (as opposed to using it as one of the discharge gases), and they also performed OES on the afterglow to determine the constituent species. When CO_2 was injected into the afterglow of an Ar/N_2 discharge, no C_2 Swan band emission was detected, indicating a lack of CO_2 dissociation. In the case when CO_2 was used as a discharge gas, the inlet stream was diluted with Ar, similar to the work of Liu et al. [20]. Under these experimental conditions, C_2 Swan band emission was observed in the afterglow (indicative of CO_2 dissociation) and the CO_2 conversion doubled from 35% to 70%. The authors attributed this increase to the combination of plasma-based CO_2 dissociation and RBR in the carbon bed. It should be noted however that the use of Ar as a co-reactant will incur further costs and require additional separation stages downstream to isolate the CO produced.

Huang et al. [22] demonstrated the first implementation of a post-plasma carbon bed with a gliding arc (GA) plasma reactor. The authors initially characterised their rotating GA in the absence of carbon, capturing the ignition, elongation, extinguishing and re-ignition cycle typical to GA discharges using a high-speed camera and voltage/current probes. The frequency of this cycle rose while the plasma length shortened as a function of increasing flow rate, due to the amplified convective heat transport at the higher flow rate. In the presence of carbon, the peak CO_2 conversion improved from ca. 7% to 21%, however at the expense of EE, which lowered from 36% to 24%. The observed reduction in EE occurs because the optimum flow rate for conversion when biochar is present is lower than in the empty reactor case. The authors attributed this

peak shift to the mesh covering of the outlet of the reactor, which visually decreased the afterglow volume.

Zhang et al. [23] investigated the use of a warm plasmatron reactor operated in pure CO_2 in combination with a carbon bed. They compared the efficiency of a fixed and fluidized carbon bed, in addition to researching the implemented biochar properties. Upon comparison of the beds, they observed that the fixed bed performed better in terms of conversion and EE under almost all flow rates investigated. As similar SEI values (hence relatively equal plasma-based power at a fixed flow rate) were recorded at each flow condition, they attributed the difference to a combination of a lower measured gas temperature and a higher recombination rate for the produced CO and O_2 due to a longer pathway prior to reacting with the biochar in the fluidised bed. In terms of biochar properties, the main factor identified by the authors was the carbon content – materials with higher carbon content (determined by elemental analysis) performed the best. Interestingly, when comparing a single biochar source pyrolyzed at three different temperatures, the results indicated both that a higher carbon content was beneficial, but also that increasing the surface area of the material by an order of magnitude did not affect the performance to a similar level.

A previous work from our group conducted by Girard-Sahun et al. [18] implemented a combined experimental and modelling approach to provide more insight into their results. In addition to this two-pronged approach, they also developed a silo system to enable continuous carbon feeding and replenishment of the bed throughout the course of an experiment. The experiments were carried out using a gliding arc plasmatron (GAP) reactor and an AC power supply to reduce electrode degradation. Upon ignition in the presence of carbon, the authors recorded peaks of CO production and CO_2 destruction, reaching a conversion up to 13%. However, after a few minutes this value dropped to around 5%, lower than the steady-state value of 8% obtained in the absence of carbon. This reduced performance indicates that the silo system was not working efficiently. Their quasi-1D model suggested that this transient behaviour in the presence of carbon was due to the oxidation of the surface of the carbon particles. Initially, this produces CO via the RBR, but subsequent coverage of oxygen complexes favours the production of CO_2 instead [18], which resulted in a lower conversion than the benchmark case. The authors suggest this oxygen coverage can be limited by providing a higher bed temperature, either through additional heating or by supplying more power to the system, but such experiments were not carried out in their study..

Most recently, Wu et al. [24] coupled an atmospheric pressure MW plasma to a carbon bed, utilising Ar and CO_2 as input gases. They initially characterised the afterglow using OES, observing a higher intensity of C_2 Swan band emission with increasing power due to improved CO_2 dissociation in the larger plasma volume. Interestingly, they also spatially defined the axial lifetime of C_2 and atomic O species, demonstrating a near-complete removal of both ca. 3 cm downstream from the mounting hole of their waveguide. Upon introducing biochar to a fixed carbon bed downstream, the authors first tested the effect of the Ar dilution on its performance, observing a near-linear rise in absolute CO_2 conversion with increasing fraction of Ar. The EE peaked at 30%–40% Ar and decreased at higher fractions owing to the imbalance of energy supplied to Ar ionisation and CO_2 dissociation. Finally, they tested char from two different sources (coconut shell and bamboo), achieving an optimum absolute CO_2 conversion of 75% for a corresponding EE of 30% with the smaller coconut shell char. However, the effective CO_2 conversion, accounting for the fraction of CO_2 in relation to the total feed gas mixture (see further), was 60%.

It is clear that previous works on the topic have extensively investigated the effect of (i) process parameters (temperature, SEI), (ii) the nature and type of carbon materials, and (iii) the nature of carbon bed (fixed or fluidized) for this process. To date, however, the insights into the best design of fixed carbon beds are clearly lacking. In this work, we focus on the reactor setup and effect of carbon bed design on the efficiency of the process, namely the effects of bed length and additional bed insulation. To this end, we tested three different carbon beds with the same type of activated carbon at two distinct SEI values in a GAP reactor, and we demonstrate the optimum functioning of the silo system. The effect of additional pre-heating of the external silo, also to overcome the limitations encountered by Girard-Sahun et al. [18] was also investigated. In addition, we present an updated method for calculating the EE of the process, based on the work of Zhang et al. [23], clearly elucidating the contribution of direct CO_2 dissociation from the plasma and of the RBR at the carbon bed to the EE of the process using simple process outputs.

3. Experimental

The experiments carried out in this work were conducted using a gliding arc plasmatron (GAP) developed by Nunnally et al. [25] and used in previous works within our group [10,11], including with a post-plasma carbon bed [18]. A basic schematic of the reactor setup configurated with an external silo is outlined in Fig. 1(a). While the same reactor was used, there were some notable differences to the setup used in previous works within our group. The material of the electrode insulation pieces was changed from Teflon to ceramic (top piece Macor, bottom piece alumina) to enable longer operation times and higher currents to flow through the reactor. This is important to realize a higher carbon bed temperature, and thus for improving the effect of the carbon bed. A detailed schematic of the cathode and anode housing, including the ceramic insulation piece, is shown in Fig. 1(b). To increase the contribution of the endothermic RBR, the power supply unit (PSU) was also changed from AC to DC (Technix, SR12KV-10KW) to increase the gas temperature of the effluent [26].

Pure CO_2 (99.999%, Air Liquide) was supplied to a single gas inlet connected to a swirl ring containing six tangential inlets, and the flow rate was controlled using a mass flow controller (MFC) (Bronkhorst, F-201A). The outlet mixture was analysed using non-dispersive infrared (NDIR) detectors for CO and CO_2 (SmartGas, FLOW-EVO) and an optical sensor for O_2 (Pyroscience, FDO2). A small-scale cyclone separator and in-line filters were installed between the reactor and analytics/exhaust to remove solid dust particles and prevent contamination of the sensors (Fig. 1a).

The negative polarity current-controlled source was connected to the high-voltage electrode while the reactor body was grounded. The voltage was initially set to 12 kV to initiate the gas breakdown at the shortest distance, while the working voltage was free to vary according to the plasma length and resistivity (typically 1–1.5 kV). The voltage differential across the plasma was measured using a high-voltage probe (Tektronix, P6015A) connected to the cathode and ground connection. The current was measured using a current sense resistor (2 O) connected to a digital oscilloscope (Keysight, DSOX1102A) in addition to the high-voltage probe. A ballast resistor (200 O) was placed in series between the PSU and reactor to increase the resistive load detected by the PSU, resulting in a more stable discharge. The plasma typically exists in a takeover mode [27,28], manifested as quasi-periodic peaks in current and voltage. An example oscillogram demonstrating these fluctuations in voltage and current is shown in the supporting information (Fig. S1). A high SEI value around 6.8 kJ/L (1.7 eV/molecule) and a low SEI value around 3.7 kJ/L (0.92 eV/molecule) were applied to each of the different bed configurations.

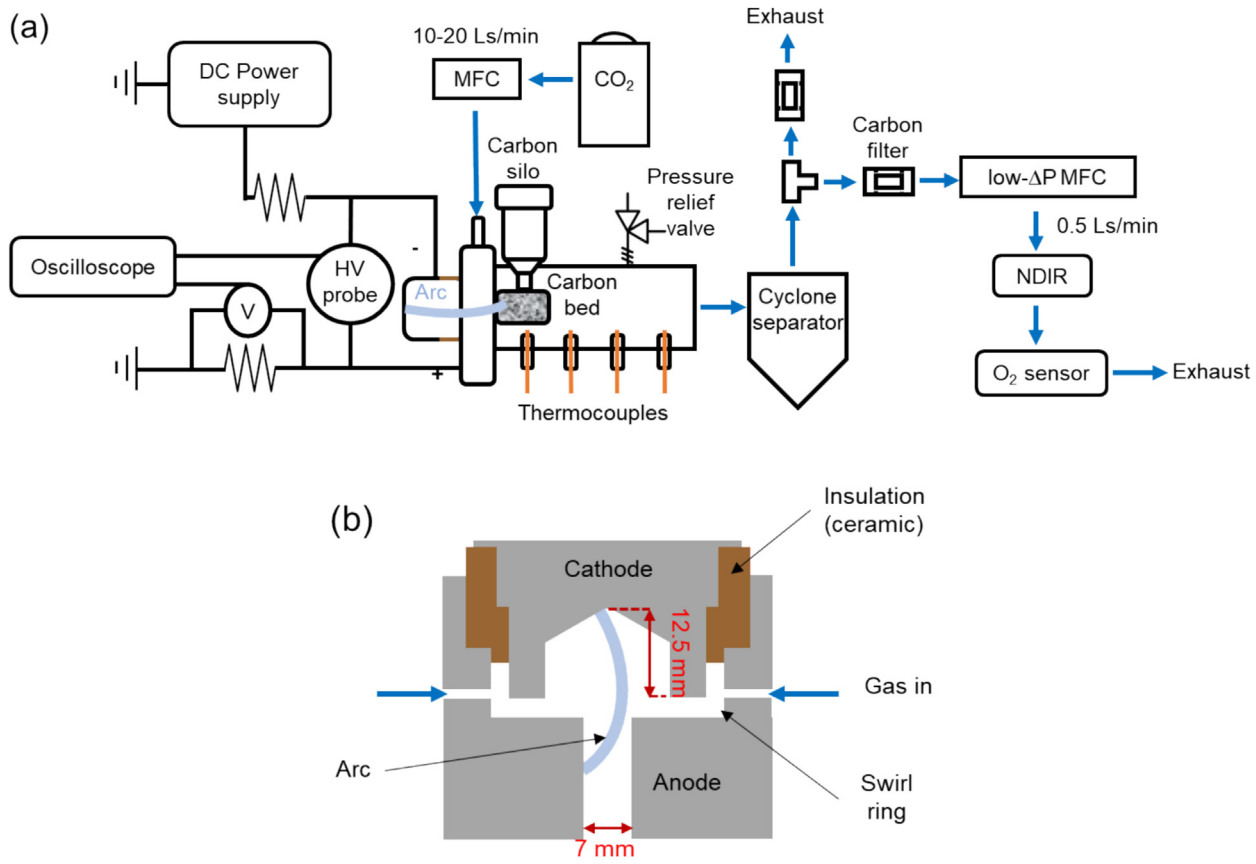

Fig. 1. Representative (a) reactor setup schematic shown for a configuration utilising external silo and (b) detailed cathode/anode coupling showing insulation and swirl ring (with six tangential gas inlets).

In each experiment, 80 g of steam-activated carbon pellets (Norit ROW, 0.8 mm diameter) were loaded into the silo and bed. The 'long bed' outlined in Fig. 2(b) is the same as used by Girard-Sahun et al. and was coupled to the previously developed silo system, but now properly functioning (see below, Sections 5.1.1 and 5.5). The 'short bed' (Fig. 2b) has an identical design and diameter as the long bed, differing only in the length, which was approximately halved (long bed = 35 mm, short bed = 15 mm), with the purpose of heating a smaller volume of carbon to an adequate temperature to facilitate the RBR. This bed was operated with the same external silo as the long bed. The third design ('insulated bed', Fig. 2c) differs from the previous two as it contains an elongated anode tube and an additional layer. The elongated anode tube was implemented to reduce arc disruption of fresh carbon flowing from the silo into the bed and the extra layer requires the hot effluent gas to pass through the carbon bed and back around it, creating an insulating layer of high-temperature gas. The additional layer was implemented to maintain and, more importantly, to increase the average bed temperature, an effect that was highlighted by our previous modelling study as key to improving carbon bed performance [18].

The temperature along the length of the reactor was monitored using a digital thermometer (Omega, HH520) with thermocouples (K-type) inserted into the exhaust chamber at four locations (see Fig. 1a). Direct measurement of the temperature inside the beds was not possible as the temperature within the beds was above the limit of K-type thermocouples (>1260 °C).

To test the effect of pre-heating the external silo coupled to the short and long beds, a heating tape (Isopad, TD7000) was wrapped around the filled stainless steel silo (Fig. S2). This line was heated to a temperature of 150 °C and maintained at this value for at least 4 h. Once this pre-heating time had elapsed, the experiment was started with the heating tape remaining in place.

4. Metrics calculation and analysis

Our group previously emphasized the importance of uniform and precise methods for calculating process metrics, including those for CO_2 plasmolysis [29]. Here, we calculated the conversion, SEI and EC according to formulae derived therein. To accurately calculate the conversion, the volumetric flow rate at the outlet (Q_{out}) is required. In this work, we utilise the oxygen balance to determine Q_{out} in the same manner as Zhang et al. [23]. In their work, they compared the calculated flow rate to the measured one using a volumetric flow meter and observed good agreement for their experimental conditions. As such, Q_{out} (L/min) was calculated by:

$$Q_{out} = \frac{2 * Q_{in}}{\left(2 * (\gamma_{CO_2} + \gamma_{O_2}) + \gamma_{CO}\right)} \quad (4)$$

where Q_{in} is the volumetric flow rate at the inlet (L/min) and γ is the fraction of the component indicated in the subscript (i.e. CO_2, O_2 or CO). Using this definition, the conversion (X, %) is calculated according to:

$$X = \frac{Q_{in} - (Q_{out} * y_{CO_2})}{Q_{in}} * 100 \quad (5)$$

wherein 100 is the conversion from fraction to percentage (%). The SEI (kJ/L) is the ratio of power to flow rate, defined as:

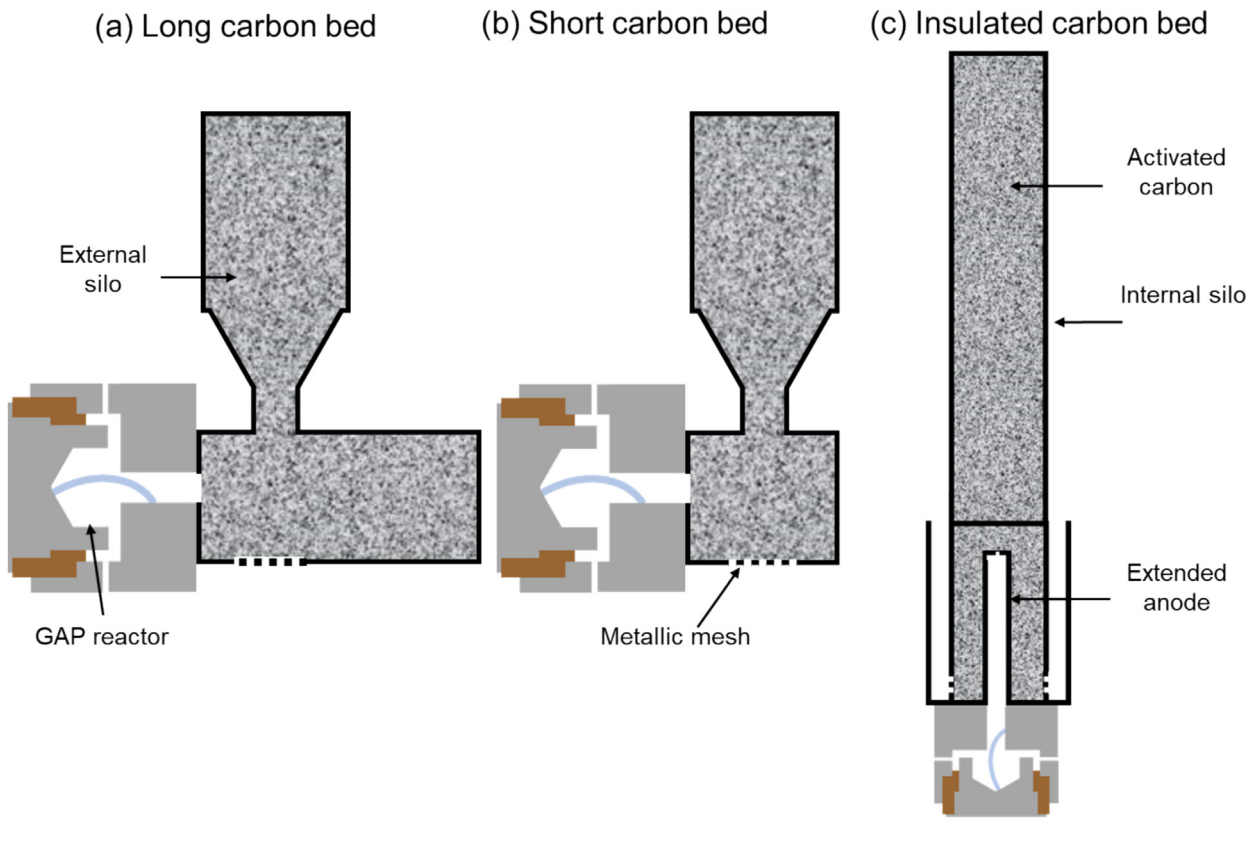

Fig. 2. Illustration of (a) long, (b) short, and (c) insulated carbon beds with coupled silos.

$$\mathrm{SEI} = \frac{P}{Q_{\mathrm{in}}} \times 60 \tag{6}$$

In this equation, 60 is the number of seconds per minute (s/min) and P is defined as the plasma-deposited power (kW) which does not account for power losses incurred from the power supply or the ballast resistor. While we acknowledge the importance of reporting the plug power to assess the industrial viability of plasma processes [30], in this work we focus on the plasma power to enable direct comparison to other works in literature, which almost exclusively report plasma power. The units of SEI can be set as kJ/L, kJ/mol, and eV/molecule, the conversions for which are shown in Eqs. (7) and (8).

$$\mathrm{SEI[kJ/mol]} = \mathrm{SEI[kJ/L]} \times V_{\mathrm{m}} \tag{7}$$

$$\mathrm{SEI[eV/molecule]} = \mathrm{SEI[kJ/mol]} \times \frac{6.242 \times 10^{21}}{N_{\mathrm{A}}} \tag{8}$$

where V_{m} is the standard molar volume (24.06 L/mol at 293 K and 1 atm, i.e. standard EU = normal USA [29]), 6.242×10^{21} is the amount of electron volts per kilojoule (eV/kJ) and N_{A} is Avogadro's constant (6.022×10^{23} molecule/mol). It should be noted that careful consideration should be given to the value elected for V_{m}, as this varies depending on the definition of reference temperature and pressure.

As mentioned in the Introduction, several previous works have attempted to define the EE when utilising a post-plasma carbon bed for improving CO_2 conversion. Since two reactions of CO_2 conversion take place, this metric requires the use of two standard reaction enthalpies ($\Delta H_{\mathrm{r}}^{\circ}$), namely that of CO_2 dissociation ($\Delta H_{\mathrm{r}}^{\circ} = 283$ kJ/mol) and of the RBR ($\Delta H_{\mathrm{r}}^{\circ} = 172.5$ kJ/mol).

Huang et al. [22] and Zhang et al. [23] derived contribution equations for each reaction based on the oxygen balance (Section S2). However, problems arise within these formulae when the detected O_2 fraction at the outlet becomes zero (as is the case in our work and most other post-plasma carbon bed works). In this scenario, the contribution of the plasma-based dissociation becomes zero, meaning the RBR becomes responsible for the entirety of the CO_2 conversion obtained. Since the enthalpy of the RBR is lower than that of CO_2 dissociation, this leads to an underestimation of the EE.

In reality, a significant part of the measured CO_2 conversion is due to the initial plasma-based dissociation, which cannot be captured by the formulae derived by Huang and Zhang et al. Hence, we propose an alternative set of equations, based on the results obtained using an empty bed at the same SEI as recorded in a corresponding filled bed experiment. By using these values, the relative contributions can be calculated as follows.

$$\alpha_{\mathrm{Dissociation}} = \frac{X_{\mathrm{empty}}}{X} \tag{9}$$

$$\alpha_{\mathrm{RBR}} = 1 - \alpha_{\mathrm{Dissociation}} \tag{10}$$

where α is the unitless contribution factor (between 0 and 1), with the subscript defining the pertinent reaction, X_{empty} is the conversion obtained in an empty bed (%) and X is the conversion obtained in the presence of carbon (%). These equations require two key assumptions, namely:

1. The overall conversion of CO_2 based on plasma-based dissociation is constant in the presence and absence of carbon.
2. The reaction of produced O_2 with carbon results in only the formation of CO and not CO_2.

We tested the first assumption by packing an inert material (Al_2O_3 spheres) into the insulated bed and comparing the conversion to the empty bed result. The deviation between the inert packed and empty insulated bed conversions was small enough (8.8% and 8.2%, respectively) to consider this assumption valid. The same test could not be conducted in either the short or long bed as the plasma afterglow is in direct contact with the material in these configurations, resulting in damage and decomposition of the materials. The second assumption appears to be valid provided the CO_2 concentration detected does not exceed that detected during the empty bed experiments. If the opposite is assumed (i.e. formed O_2 reacts with solid carbon to form CO_2), the conversion would remain the same, but the EE would deviate slightly, as illustrated in the numerical example in SI (Section S3).

Thus, the equation for the EE (%) defined by Huang et al. [22] and Zhang et al. [23] can be utilised with these new definitions for the contributions.

$$\mathrm{EE} = \frac{X \times (\alpha_{\mathrm{Dissociation}} \times \Delta H^{o}_{\mathrm{r,Dissociation}} + \alpha_{\mathrm{RBR}} * \Delta H^{o}_{\mathrm{r,RBR}})}{\mathrm{SEI}} \quad (11)$$

where $\Delta H^{\circ}_{\mathrm{r,\,Dissociation}}$ is the standard reaction enthalpy for CO_2 dissociation (283 kJ/mol), $\Delta H^{\circ}_{\mathrm{r,\,RBR}}$ is the standard reaction enthalpy for the RBR (172.5 kJ/mol), α is the contribution factor with the subscript defining the pertinent reaction and SEI is defined in kJ/mol.

Another, more simplified process efficiency metric is the EC (MJ/mol). This parameter combines the conversion and SEI parameters into a quantifiable measure of the energy expenditure of the process. In situations where determining the pertinent reaction pathways and their relative contributions to EE can be difficult, EC is a more useful metric as it provides a simple number without the need for assumptions or detailed reaction pathway analyses. It is defined as:

$$\mathrm{EC} = \frac{\mathrm{SEI} * V_{\mathrm{m}}}{X/100} \times \frac{1}{1000} \quad (12)$$

In this equation, the denominator 100 (%) is to retrieve the conversion as a fraction and 1/1000 is the ratio of MJ to kJ (MJ/kJ). As X is the percentage conversion of CO_2 (%), the EC is technically represented as MJ/mol CO_2. For simplicity, we will refer to the unit of EC hereafter as MJ/mol. To convert the units of EC from MJ/mol to eV/molecule, the following formula can be used:

$$\mathrm{EC[eV/molecule]} = \mathrm{EC[MJ/mol]} \times \frac{6.242x10^{24}}{N_{\mathrm{A}}} \quad (13)$$

where 6.242×10^{24} is the amount of electron volts per megajoule (eV/MJ). In the presence of carbon, the concentration of O_2 remained negligible (<0.1 vol%) in each experiment. Once the carbon is fully consumed, the O_2 concentration rises (Fig. S3) marking the time point after which the experiment was concluded. In addition to this, the CO and CO_2 profiles were temporally stochastic in nature, especially with the short and long bed configurations. Such profiles make the calculation of conversion more difficult than steady-state systems. The volumetric outflow (Q_{out}) and conversion profiles for each repeat were calculated directly using these oscillating profiles, with an average conversion value determined from three of these oscillating conversion profiles during the pseudo-steady state that appeared after some duration. An example of the oscillating concentration and conversion profiles is also shown in SI (Fig. S3), with the latter highlighting the pseudo-steady state region.

Due to these oscillations, the standard deviation of these metrics appears large when plotted in the following figures. For the EE and EC, the error was propagated using the standard deviations and partial derivatives (with respect to their variables) of the conversion and SEI values.

5. Results and discussion

For each stage in this investigation, we examined and compared the effect of two different SEI values (i.e. ratio of power to flow rate) on the conversion and energy metric performances. In each case, the flow rate was fixed and the SEI values between the beds were aligned by varying the power delivered by the PSU. For this purpose, the current was adjusted and the voltage was allowed to vary in response to the resistivity of the system. For the high and low SEI conditions, the flow rate was set to 10 and 20 L/min, respectively, resulting in SEI values around 6.8 kJ/L (1.7 eV/-molecule) and 3.7 kJ/L (0.92 eV/molecule). During each experiment, less than 0.1% of O_2 was detected in the effluent stream for the duration of the experiment when carbonaceous material was present in the bed. This means the carbon bed was always effective for removing the O_2 produced by CO_2 splitting, which will lower the overall separation costs of plasma-based CO_2 splitting.

5.1. Effect of bed length

5.1.1. Conversion and concentration profiles

We investigated the effect of bed length by comparing the average CO_2 conversion obtained with the short and long beds in Fig. 3 (a and b), while the CO and O_2 concentrations for these conditions can be seen in Fig. 3(c and d).

The empty bed conversions are in the range of previously obtained results using unmodified warm plasma setups, ca. 8%–15% [9,10,31]. The conversion obtained with the empty long bed increases with decreasing SEI (from 8.4% at 6.8 kJ/L to 9.9% at 3.7 kJ/L), an effect not observed with the short empty bed and not typical for similar unmodified setups, where the conversion typically rises with SEI. The drop at higher SEI is likely due to some gas recirculation occurring further into the long bed, past the metallic mesh-covered openings where the gas exits the bed (see Fig. 2a). This yields some recombination of the products, back into CO_2, explaining the lower conversion, and this effect is enhanced at higher SEI due to the reduced convective transport along the bed at the lower flow rate. In the lower SEI case, the higher flow rate promotes the removal of the produced CO out of this high temperature recombination zone, preventing the formed CO recombining with O/O_2 and resulting in a higher CO_2 conversion of nearly 10%.

In the experiments with carbon packed into the beds, two distinctly different trends can be observed in the average conversion plots for the short and long beds, correlated to the two SEI conditions. At high SEI (i.e., lower flow rate, represented by the orange columns in Fig. 3a and b), a clear difference in conversion is present. The short bed results in a lower conversion than the long bed, with an average value of 34% compared to 41%. In both beds, CO is formed from three key overall reaction pathways with carbon outlined in the introduction (Eqs. (1)–(3)). If we assume that the combined oxygen concentration (atomic + molecular) entering the carbon bed is approximately equal to the values detected downstream in the absence of carbon (i.e. empty beds, Fig. S4a and b), we can predict O_2 concentrations in the range of 4–7 vol% entering the bed. In reality, these values may be slightly higher, as recombination of CO and O/O_2 to form CO_2 has a limited time to occur in the case of a filled carbon bed. If we conservatively estimate 10 vol% O_2 entering the bed, this will result in the production of approximately 20 vol% CO. While these values are not insignificant compared to the total CO formed (ca. 52 vol% for the short bed and ca. 58 vol% for the long bed) at this high SEI condition, it is clear that the majority of CO formed still occurs via Eq. (3), i.e., the RBR. This endothermic reaction requires temperatures above 1000 K to proceed at an appreciable rate at atmospheric pressure [18,19]. As such, a flux of heat and reactant species (CO_2) are key

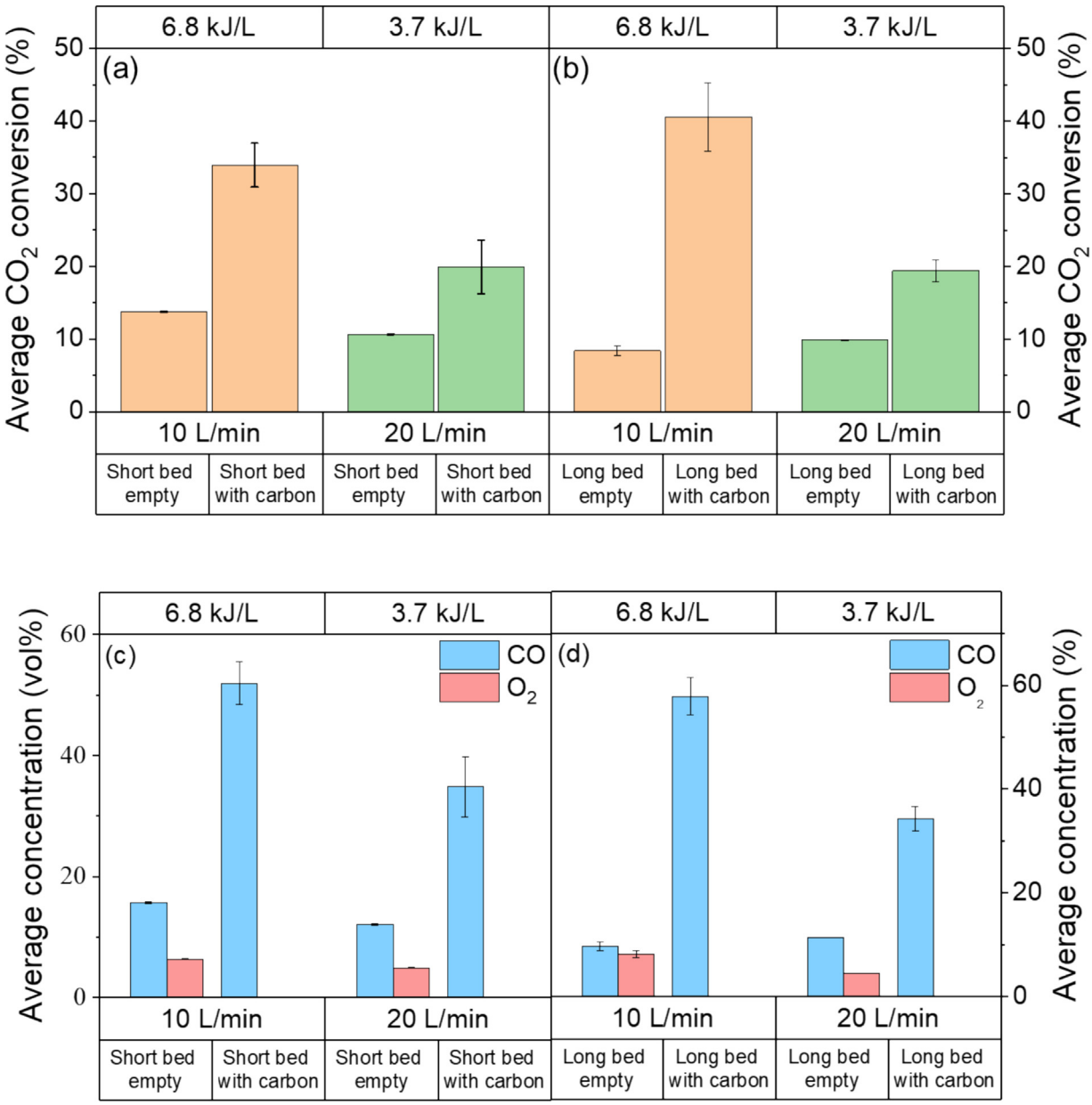

Fig. 3. Comparison of average CO_2 conversion for the (a) short and (b) long beds, as well as the corresponding CO and O_2 concentrations (c, d), when empty and filled with carbon, at high (6.8 kJ/L) and low (3.7 kJ/L) SEI values.

components required for this reaction to occur [32]. In the case of the long bed at high SEI, more heat from the plasma chamber is retained within the bed compared to the short bed. In the short bed, heat is rapidly transported out through the mesh-covered openings in the side walls, as shown schematically in Fig. 2(b). The additional length of the long bed means that some of this 'lost heat' in the short bed is transported further into the bed, heating the carbon and accelerating the RBR. In addition, the diffusive flux of CO_2 to the surface of the solid carbon pellets is higher in the long bed compared to the short bed at this SEI condition, as the extra volume allows for more carbon to be packed and an increased total surface area exposed to the high temperature gas stream. Hence, at high SEI, the long bed clearly performs better than the short bed, for the above explained reasons.

Interestingly, the difference in conversion between the beds in the presence of carbon diminishes with decreasing SEI, as represented by the green columns in Fig. 3(a and b). Under these conditions, the short bed results in an average conversion of 20% compared to 19% for the long bed. As mentioned previously, the SEI reduction is achieved by increasing the flow rate and matching the power between the setups. This suggests that the flow rate becomes the dominant parameter at lower SEI values, reducing the effect of bed length variation on the process. As such, the convective heat transport out of both beds becomes approximately equal, resulting in similar amounts of carbon at the same temperature. The temperature at the carbon surface and in the gas phase further into the long bed likely reaches a lower value compared to the high SEI case, decreasing the rate of the RBR in this section of the bed. In this scenario, the first portion of the long bed is acting as the primary site for the RBR, with the length of this site being akin to the total length of the short bed. In addition, as the flow rate increases, the diffusive contribution of species flux will

decrease in favour of convective transport out of the bed, reducing the significance of this parameter in the long bed and aligning the resulting conversion in the two beds.

For all SEI conditions applied to either the short or long bed in the presence of carbon, complete oxygen removal was achieved for the duration of the run (Fig. 3c and d). This is further highlighted in the plot of species concentrations detected at the outlet (Fig. S3a), wherein the detected O_2 concentration only rises above 0% when the CO and CO_2 concentration decrease and increase, respectively. This change occurred when over 97% of the carbon was converted and the experiment was concluded soon after (Table S1).

In summary, the best results are obtained for the long bed at high SEI, reaching a maximum CO_2 conversion of 41% (see Fig. 3b). This improvement is approximately five-fold when compared to the long bed in the absence of carbon at this condition (8.5%). Even more, the CO concentration increases from about 10% (without carbon) to nearly 60% at these conditions, a near six-fold improvement. A near-complete removal of O_2 produced from the plasma-based dissociation of CO_2 was observed during each experiment with carbonaceous material present in the bed (Fig. S3c and d). Importantly, the silo system, which did not work well in our previous work [18], now clearly functions efficiently, both due to the higher SEI achieved and the higher temperature realised within the bed (above the limit of K-type thermocouples, 1260 °C) due to the use of a DC power supply (see Section 5.5 for further comparison between the works). This efficient operation allows for carbon consumed by oxidation (Eqs. (1) and (2)) and the RBR (Eq. (3)) to be replenished and the process to run continuously until the majority of the 80 g of carbon loaded is consumed (>97%). Obviously, if the silo capacity would be increased, so too would the duration of the process and sustained high conversion and EE. A theoretical limit to said silo increase is correlated to ash accumulation in the bed, which would eventually interrupt the carbon replenishment process. However, ash accumulation in this study was minimal and we do not foresee this as an issue under these specific experimental conditions (i.e. SEI values, bed length, carbon material).

5.1.2. Energy metrics

The energy performance of the short and long beds, in terms of both EE and EC, is compared in Fig. 4(a and b).

Fig. 4(a) shows the EC and EE obtained with empty and filled short bed, at the high and low SEI conditions. In general, the energy metrics greatly improve in the presence of carbon. For example, the EE at high SEI increases from 27% to 41% in the presence of carbon. This improved value is in line with the EE obtained at low SEI in the absence of carbon (40%), but the EE rises further to ca. 51% at this low SEI with carbon present. If we look at the same data points for EC, the same effect is realised at high SEI, with the EC decreasing more than two-fold from 1.03 MJ/mol for the empty bed to 0.49 MJ/mol for the packed bed. Interestingly, the alignment between the low SEI empty bed and high SEI filled bed is no longer retained, with the filled bed at high SEI achieving a lower EC than the empty bed at low SEI (0.71 MJ/mol). This discrepancy is a prime example of the misalignment between EE and EC that can occur in complex reaction systems. As mentioned previously, we advise the use of the simpler and more straightforward EC as the key energy metric, which indicates that the addition of carbon has a highly beneficial effect on the energy performance. The lowest EC with the short bed is obtained in the presence of carbon at low SEI, reaching 0.41 MJ/mol.

The EE and EC values obtained in the absence and presence of carbon in the long bed are shown in Fig. 4(b). The empty bed results align well with our previous results [18], showing an increase in EE (from 15% to 36%) and a drop in EC (from 1.96 to 0.79 MJ/mol) as a function of decreasing SEI. The high SEI empty long bed condition results in the highest EC of all conditions examined. Upon introduction of carbon, the energy performance improves significantly for both SEI conditions. The most dramatic improvement occurs at high SEI, with the EE increasing from 15% to 51% and the EC markedly decreases from 1.96 to 0.41 MJ/mol. Interestingly, the EE improves only slightly with decreasing SEI in the presence of carbon, rising to a value around 54%. As the propagated error bars of the EE are quite large, these values can be considered approximately equal. This aligns with the resulting EC, with the value of 0.43 MJ/mol obtained at the lower SEI condition falling within the error of the high SEI result. Both energy metrics indicate that the effect of decreasing SEI has no significant impact on the energy performance of the long bed.

In summary, in combination with the conversion results of Fig. 3(b), the long bed filled with carbon produces the best results in terms of both optimum conversion (41%) and EE/EC (51% and 0.41 MJ/mol, respectively) at the high SEI of 6.8 kJ/L.

When comparing between the short and long bed in the presence of carbon, the EE for the long bed is higher (51%) than for the short bed (41%) at high SEI. This difference is due to the higher

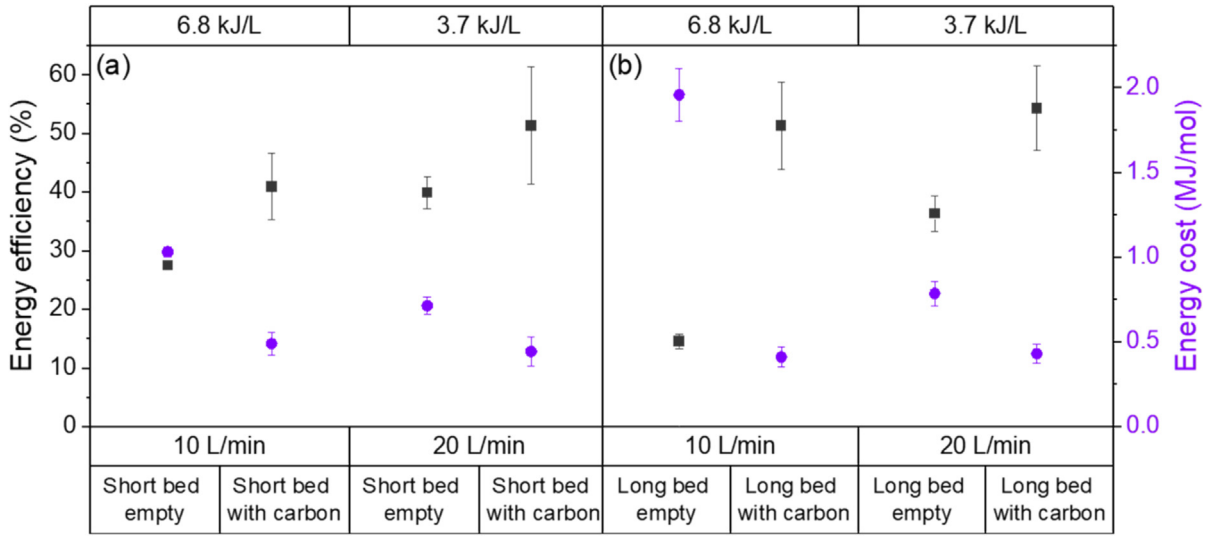

Fig. 4. Comparison of energy cost and energy efficiency for empty and filled (a) short and (b) long beds at high (6.8 kJ/L) and low (3.7 kJ/L) SEI values.

conversion at high SEI using the long bed (Fig. 3b). Interestingly, the relative contributions of the plasma-based CO_2 dissociation and the RBR to the EE vary significantly between the two beds at high SEI (Table S2). The conversion of 14% obtained with an empty short bed is greater than with an empty long bed (8.4%) (Fig. 3a and b), meaning $\alpha_{Dissociation}$ in the EE calculation (Eq. (11)) is also greater for the short bed. This value lies around 0.4 for the short bed compared to just 0.23 for the long bed. As the enthalpy of CO_2 dissociation is greater than the reaction enthalpy for the RBR (283 vs. 172.5 kJ/mol), a higher contribution factor for CO_2 dissociation ($\alpha_{Dissociation}$) leads to a higher EE of the short bed at high SEI. At low SEI, the similar conversion and contribution values for both beds result in near-equivalent EE values of 51% and 54% for the short and long bed, respectively.

As highlighted previously, EC is a more straightforward and simpler metric for determining the relative energy performance of such a complex reaction system. At high SEI, the results mirror those obtained for EE; the short bed configuration is less efficient at utilising the power deposited into the plasma when compared to the long bed. The short bed reaches an average EC of 0.49 MJ/mol, compared to 0.41 MJ/mol for the long bed at an SEI of 6.8 kJ/L. As this metric is solely determined by the conversion and SEI (Eq. (12)), combined with the fact that the SEI values between the beds were approximately matched, this difference in EC is solely due to the improved conversion in the long bed at high SEI. The difference in EC can thus be attributed to the improved heat retention and species flux to the surface of the solid carbon in the long bed, as described above. At low SEI, the EC for both configurations approach similar values, i.e., 0.44 and 0.43 MJ/mol for the short and long bed, respectively. These energy metrics clearly indicate and reinforce our finding that the bed length is not a key parameter in determining the performance of a post-plasma carbon bed below a certain SEI threshold, when heat and species convective transport becomes the dominant factor in determining the bed efficiency. However, bed length is an important design parameter to consider at high SEI, due to the reduced convective heat and species transport out of the bed at this condition. Indeed, high SEI facilitates a higher bed temperature, promoting the RBR and enabling an EC minimum of 0.41 MJ/mol.

5.2. Effect of bed insulation

In order to utilise the heat produced in the plasma downstream (post-plasma), we designed an insulated carbon bed with the specific aim of retaining residual heat, which is otherwise lost to the environment around the reactor. The time evolution profiles of CO_2 conversion obtained during a single run using the short, long and insulated beds are plotted in Fig. 5. The average conversion values, the produced CO and O_2 concentrations, EE, and EC for the insulated bed are compared in the supporting information (Figs. S4 and S5).

A noticeable difference in the conversion profiles can be seen in Fig. 5, as the oscillations present in the short and long bed plots are markedly reduced in the plot for the insulated bed. The oscillation damping observed may be the result of two key differences between the bed configurations. Firstly, the insulated bed design incorporates the carbon feeding silo inside the reactor exhaust, meaning that the high-temperature gas exiting the reactor/carbon bed must also flow past the silo prior to exiting the reactor setup. This design feature leads to heating by the gas stream of the silo and carbon stored within. Essentially, this manifests as a heating system for the carbon loaded into the silo, utilising the "waste" heat from the plasma that would otherwise be released passively. Secondly, the insulated bed is designed with an anode extension (Fig. 2c), meaning that the arc and its afterglow are not continuously impacted and interrupted by fresh carbon entering the bed,

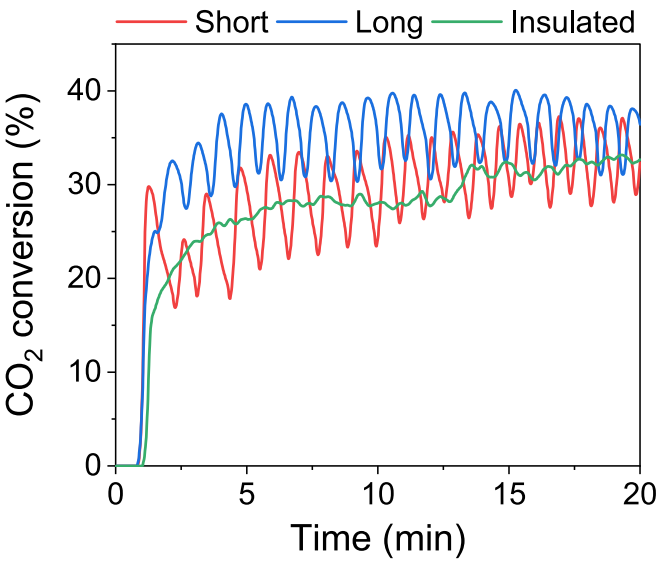

Fig. 5. Example conversion profiles obtained for the short, long and insulated beds, at SEI of 6.8 kJ/L. The fluctuations observed for the long and short beds are due to cold carbon entering the bed (see detailed explanation in the text).

as may be the case with the short and long beds. The former hypothesis of heating the silo and carbon is tested and described in section 5.4 below (Effect of heated silo). An in-depth analysis of the conversion and energy metrics obtained with the insulated bed can be found in the supporting information (Section S4).

5.3. Performance comparison of the different beds

A comparative overview of the EC versus conversion for all beds, both empty and filled, at low and high SEI can be seen in Fig. 6.

Under every experimental condition examined, the addition of carbon resulted in a significant improvement to the conversion whilst simultaneously decreasing the EC. At the low SEI condition (circles), the EC and conversion without carbon for all three beds was approximately equal (ca. 0.75 MJ/mol and 10%). This trend was maintained in the presence of carbon, with each bed resulting in a lower EC around 0.5 MJ/mol and a corresponding improved CO_2 conversion in the range of 17% to 20%. The high SEI condition (squares) produced a greater difference between the beds, both

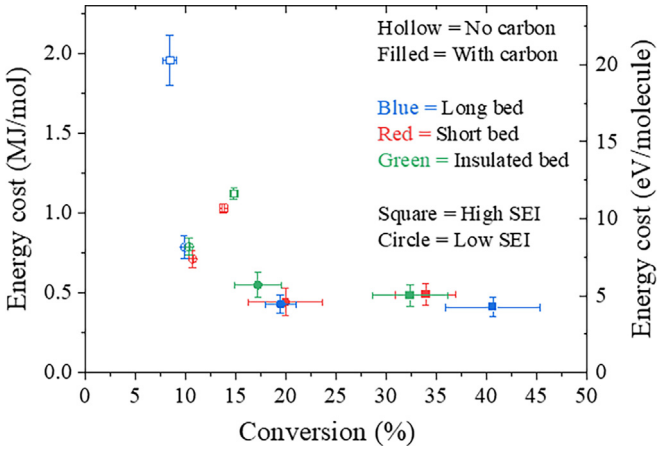

Fig. 6. Comparison of energy cost versus conversion for long (blue), short (red), and insulated (green) beds with carbon (filled symbols) and without carbon (hollow symbols) for the two experimental SEI conditions (low SEI = squares, high SEI = circles).

with (filled) and without (hollow) a carbon loading. The short (red) and insulated (green) beds performed approximately in-line with each other, resulting in halving of the EC from ca. 1 to 0.49 MJ/mol in the presence of carbon. This improved energy performance was accompanied by a more than two-fold increase in conversion, from ca. 14% to 34%. As highlighted in the in-depth analysis of the performance of the insulated bed (SI, Section S4), the insulated bed volume and length is comparable to that of the short bed. This similarity likely results in approximately equal heat and species flux into and out of the bed, resulting in the alignment of EC and conversion between these two beds. The largest improvement, which coincides with the best results obtained in this study, occurred at high SEI (squares) for the long bed (blue). The highest EC and lowest conversion were realised in this bed in the absence of carbon (ca. 2 MJ/mol and 8.5% respectively). This poor performance was drastically improved once carbon was loaded into the bed, with the EC reducing more than four-fold to 0.41 MJ/mol (ca. 4.23 eV/molecule) and the conversion increasing nearly five-fold to 41%. Evidently, the implemented post-plasma carbon beds were effective for reducing the EC of the process in addition to increasing the conversion. Importantly, this effect was amplified at high SEI, with the long bed (blue) outperforming the short (red) and insulated (green) beds for both of the key metrics. This insight suggests that carbon bed length should be proportional to the input variable of SEI, especially at higher SEI values.

5.4. Effect of a heated silo

The absence of large oscillations of the process performance (as reflected by the CO_2 conversion profile in Fig. 5) when using the insulated carbon bed leads to the hypothesis that said oscillations are caused by the cold carbon entering the bed from the external, non-heated silo, in case of the long and short carbon beds (see Fig. 2a and b, respectively). As such, we applied external heating to the silo to test this effect. Fig. 7 shows an example of conversion profiles obtained with the long bed at high SEI (6.8 kJ/L).

The dramatic oscillations present without pre-heating (blue) are significantly reduced in the case of pre-heating the external silo (black). While the profiles differ greatly, the average conversion values remain virtually constant within the steady-like state timeframe (Fig. S3b), with a value around 39% for the pre-heated case versus 40% for the non-preheated silo. Naturally, the EE and EC values also remain approximately equal (ca. 46% and 0.49 MJ/mol, respectively, for the heated scenario).

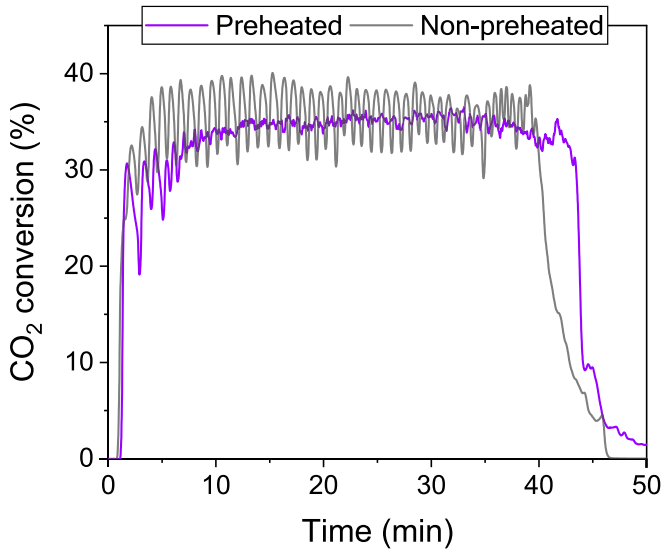

Fig. 7. Conversion profiles for the long bed with and without pre-heating of the external filled silo at high SEI (6.8 kJ/L).

In actuality, reactor design improvements with heat recovery from the post-plasma chamber could be applied to the silo to allow for energy cost calculation directly from the plug or plasma-deposited power (such as in the insulated bed design). However, at our initial experimental stage, we should include the energy required to heat the carbon in the silo into the energy cost of the process to allow accurate metrics estimation (Eq. (14)).

$$Q = m \times C_p \times \Delta T \quad (14)$$

Q (J) is the heat required to change the temperature of a substance by the amount equal to ΔT (K), m is the mass of the substance (kg) and C_p is the specific heat capacity (J/(kg K)). If we assume that the 80 g of carbon in the silo reaches a temperature of 150 °C (to which the heating tape was set), with the heat capacity of carbon as 1.1 J/g °C and the molar mass of activated carbon equal to 12.01 g/mol, then the energy required amounts to approximately 1.7 kJ/mol. This small figure lies within the error margin of the EC calculation for the process, indicating the minor impact it has on the final EC figure.

Even with these considerations, some minor oscillations in the pre-heated conversion profile remain, indicating that the heated silo is the major (but not the sole) reason for the insulated bed removing the oscillations observed with the short and long counterparts. The disruption of the arc and afterglow by fresh carbon entering the bed is likely the secondary, less significant cause of the oscillations. In the current short and long bed designs, the connection between the bed and the silo is positioned close to the reactor outlet, meaning that the carbon dropping into the bed falls directly into the path of the arc/afterglow. Unfortunately, this disruption cannot be determined from the monitored electrical properties of the arc (e.g. using the voltage to determine the change in the arc length) due to the stochastic nature of the takeover mode in which the arc operates (Fig. S1). Further clarification of this effect could be achieved by redesigning the bed and external silo coupling to be as far into the bed as possible from the reactor outlet (Fig. S6).

Overall, although the insulated carbon bed and its integrated, inherently heated silo perform slightly worse than the optimum long bed used in this study, their design and employment aided the identification of a simple method for reducing performance oscillations. While such oscillations are manageable industrially, they would incur additional costs at the product separation stage (e.g. requiring large buffer vessels, increased reactor container footprint). As evidenced in our work, these extra detractors can be bypassed by implementing simple heat recovery for heating the carbon silo (either integrated or external).

5.5. Comparison with state-of-the-art

An overview of the process metrics derived from the currently available literature implementing a post-plasma carbon bed is compiled in Table 1. The conditions resulting in the highest conversion were elected as the condition of interest, with the EE and EC values taken at this condition. It should be noted that these metrics often did not align (i.e. highest conversion not obtained with the highest EE/lowest EC), unlike in our work wherein the optimum conversion (41%) and EE/EC (51% and 0.41 MJ/mol) were obtained with the same carbon bed (long) at the same SEI condition (6.8 kJ/L).

The works with over-estimated EE due to neglecting the contribution of the lower enthalpy RBR are indicated "([a])" along with those underestimating the EE due to overestimation of the RBR contribution "([b])". If data is presented in these works for the conversion in the absence of carbon, the EE has been re-calculated "([c])" to allow direct comparison with our work. If

Table 1
Overview of published post-plasma carbon bed results, compared with our work.

Entry #	Plasma reactor type	CO_2 flow rate (L/min)	Specific energy input		CO_2 conversion (%)	Energy		Ref.
			(kJ/L)	(eV/mlc)		Cost (MJ/mol CO_2)	Efficiency (%)	
1.[a]	MW plasma	10	24	5.99	40	1.44	14	Uhm et al. [19]
2.[a,d]	DC thermal plasma	26	19	4.71	95 (48)	0.94	30	Liu et al. [20]
3.[a,d]	DC thermal plasma	23	20	4.99	93 (46)	1.06	27	Li et al.[21]
4.[b]	DC GA	4	7.5	1.87	21	0.85	24	Huang et al. [22]
5.[b]	DC GAP	5	5.5	1.37	27	0.48	37 (41[c])	Zhang et al. [23]
6.[a]	AC GAP	10	3.2	0.81	13	0.62	45 (39[c])	Girard-Sahun et al. [18]
7.[a,d]	MW plasma	4.8	18	4.18	75 (60)	0.67	30 (29[c])	Wu et al. [24]
8.	DC GAP	10	6.8	1.70	41	0.41	51	This work

[a] Overestimated EE.
[b] Underestimated EE.
[c] Corrected EE in parentheses.
[d] Effective conversion in parentheses.

CO_2 was diluted with a secondary gas (e.g. Ar) "([d])", the absolute conversion is listed, with the effective conversion shown in parentheses. If V_m was not stated in the publication, the SEI was converted from kJ/L to eV/molecule assuming a standard molar volume of 24.06 L/mol (293 K and 1 atm) as used in this work.

The works of Liu et al. (Entry #2) and Li et al. (Entry #3) report energy metrics in terms of CO output, resulting in higher EE and lower EC compared to electing CO_2 as the molecule of interest. These values have been recalculated in relation to converted CO_2 to align with this and other published works.

We specifically focus on three parameters as performance criteria: (1) CO_2 conversion, (2) EC, and (3) EE (albeit more ambiguous than EC). For each of the entries shown (except Uhm et al. – no data available), O_2 was completely removed from the effluent stream in the presence of carbon, demonstrating the potential of a post-plasma carbon bed for producing an O_2-free effluent stream. In our study (Entry #8), the best results (obtained using the long bed) have improved upon the conversion as well as both energy metrics in comparison to other warm plasma setups reported in literature (Entries #1 and #4–7). In terms of SEI, the most comparable work was carried out by Huang et al. (Entry #4), wherein the authors achieved a peak conversion of 21% at an EC of 0.74 MJ/mol. We observe a near two-fold improvement in conversion and EC in our work. Girard-Sahun et al. (Entry #6) used a similar setup to the long bed configuration used in our work, albeit with an AC PSU. Our conversion is improved by more than a factor of three (from 13% to 41%), while the EC is also reduced significantly (from 0.57 to 0.41 MJ/mol). This difference is likely due to the higher SEI applied in our work, in addition to the use of a DC PSU, which enables a higher temperature within the carbon bed and facilitates an enhancement of the RBR. Moreover, we report average conversion and EE/EC values which can be maintained (within the error margins) for a notably longer plasma operation time (order of 1 h), due to the continuous supply of fresh carbon from the silo. This was not the case in the work of Girard-Sahun et al. [18], where the performance enhancement of the carbon bed was only obtained for a few minutes.

If we contrast Girard-Sahun's results with those obtained at low SEI (3.7 kJ/L) in our study, our setup still performs better, with a conversion of 19% versus 13% realised in their work. An EC comparison at these conditions supports the improvement, reaching a low EC of 0.43 MJ/mol compared to 0.57 MJ/mol achieved previously. As the SEI was approximately equal for these results, the difference arises primarily due to the PSUs used. The DC PSU in our study leads to a higher post-plasma temperature compared to the AC PSU, due to the constant electrode polarity [26], demonstrating that the type of PSU can also significantly affect the performance.

In the studies with MW plasma reactors, Uhm et al. (Entry #1) obtained a conversion similar to our work (ca. 40%), albeit with a significantly higher EC of 1.3 MJ/mol. More recently, Wu et al. (Entry #7) reported a higher (absolute) CO_2 conversion (75%) than our work, but also required an elevated EC (0.72 MJ/mol) to achieve this result. Importantly, however, this study diluted the CO_2 inlet gas stream with argon, and was thus reporting absolute conversion instead of the more correct effective conversion, which accounts for the multi-component inlet mixture [29]. The effective conversion obtained (60%) was still higher than the conversion obtained in this work due to the high SEI (18 kJ/L) applied to the MW reactor. This value is more akin to that used in thermal plasma systems (Entries #2–3), which has a positive effect on conversion but clearly sacrifices the energy performance. In contrast, our system reaches a peak conversion and minimum EC (and maximum EE) at the same SEI.

When comparing our results with those obtained using thermal plasma systems (Entries #2 and #3), a clear difference in conversion is present. Both studies required Ar dilution of the inlet CO_2 stream to operate and reported absolute conversions up to 95%, while the more correct effective conversion values were decidedly lower. For example, the effective conversions obtained by Liu (Entry #2) and Li (Entry #3) would be equal to 48% and 46%, respectively. These values are more representative of the CO_2 conversion in relation to the total inflow gas stream. Similar to the high SEI case of Wu et al., a higher EC is required to obtain these higher reported conversions.

As evidenced by the recalculated variability in EE in Entries #4–6 and the indicated overestimated EE of Entries #1–3, EE is a difficult metric to calculate accurately in a relatively complex system, such as a post-plasma carbon bed. While our recalculation and derivation addition to the work of Zhang et al. provides a more realistic overview, the metric of EC is a far more consistent definition for the energy performance of the system. This definition can only vary depending on the power measurement and the molecule of interest. In each case in the table (including our work), the power used in the EC calculation is the plasma-deposited power. A more industrially relevant power measurement would be the total power, also known as "plug power", which accounts for power requirements of the PSU, chillers and other electrical components (e.g. ballast resistors) of the system. In terms of the molecule of interest, the EC values shown in the table correspond to the molar quantity of the CO_2 input.

6. Conclusions

We presented various post-plasma carbon bed designs for enhancing CO_2 conversion. The bed length has an impact on conversion and EC at high SEI (6.8 kJ/L, 1.7 eV/molecule), with the longest bed reaching a maximum conversion of 41% with a mini-

mum EC of 0.41 MJ/mol and maximum EE of 51%. At a lower SEI of 3.7 kJ/L (0.97 eV/molecule), the short and long beds produce similar results in conversion and EC (ca. 20% and 0.43 MJ/mol, respectively). An external silo for continuous carbon supply was successfully implemented, enabling sustained high average conversion and energy metrics for extended periods (order of 1 h). The effect of additional insulation of the bed has a negligible impact on the average performance but the innovative integrated silo system implemented real-time heat recovery in the form of heating the carbon residing in the silo system. This recovery resulted in the removal of oscillations in the conversion profile, providing a more stable and consistent output to the process. Pre-heating of the external carbon silo was tested, yielding a similar smoothed conversion profile to the insulated bed and thus highlighting the importance of pre-heating the carbon prior to entering the bed/reaction zone. Furthermore, we presented an updated formula for the calculation of EE, which emphasises the variability of this metric, as also reflected by the comparison of the state-of-the-art carbon bed works. In such a scenario, Occam's razor should be reflected upon, and we therefore advocate for the use of the more straightforward metric of EC as the primary method of energy comparison between post-plasma carbon bed systems. Last but not least, we conducted an in-depth comparison with current state-of-the-art post-plasma carbon bed setups, demonstrating the drastic improvement obtained with our setup (long bed, high SEI) by achieving both high conversion (41%) as well as the lowest EC (0.41 MJ/mol) and highest EE (51%) reported to-date, that coincide at the same SEI.

CRediT authorship contribution statement

Colin O'Modhrain: Writing – review & editing, Writing – original draft, Visualization, Validation, Resources, Project administration, Methodology, Investigation, Formal analysis, Data curation, Conceptualization. **Yury Gorbanev:** Writing – review & editing, Supervision, Project administration, Data curation, Conceptualization. **Annemie Bogaerts:** Writing – review & editing, Supervision, Funding acquisition.

Declaration of competing interest

The authors declare that they have no known competing financial interests or personal relationships that could have appeared to influence the work reported in this paper.

Acknowledgments

This research is financially supported by the VLAIO-Catalisti ICON project "BluePlasma" (grant ID HBC.2022.0445), as well as by the European Research Council (ERC) under the European Union's Horizon 2020 research and innovation program (Grant Agreement No. 810182 – SCOPE ERC Synergy project) and the Horizon Europe Research and Innovation Action (Grant Agreement No. 101172766 — EffiTorch). We would also like to thank Maarten Lissens for his help in gathering the experimental data.

Appendix A. Supplementary material

Supplementary data to this article can be found online at https://doi.org/10.1016/j.jechem.2024.12.066.

References

[1] B.M. Tackett, E. Gomez, J.G. Chen, Nat. Catal. 2 (2019) 381–386.
[2] J. Gao, S. Choo Sze Shiong, Y. Liu, Chem. Eng. J. 472 (2023) 144–156.
[3] O. Gutiérrez-Sánchez, B. Bohlen, N. Daems, M. Bulut, D. Pant, T. Breugelmans, ChemElectroChem 9 (2022) e202200123.
[4] G. Wang, J. Chen, Y. Ding, P. Cai, L. Yi, Y. Li, C. Tu, Y. Hou, Z. Wen, L. Dai, Chem. Soc. Rev. 50 (2021) 4993–5061.
[5] S. Patial, R. Kumar, P. Raizada, P. Singh, Q. Van Le, E. Lichtfouse, D. Le Tri Nguyen, V.H. Nguyen, Environ. Res. 197 (2021) 111134.
[6] Y. Li, Y. Wei, W. He, Z. Tang, J. Xiong, Z. Zhao, Chin. Chem. Lett. 34 (2023) 108429.
[7] V. Longo, G. Centi, S. Perathoner, C. Genovese, Curr. Opin. Green Sustain. Chem. 46 (2024) 100893–100993.
[8] R. Snoeckx, A. Bogaerts, Chem. Soc. Rev. 46 (2017) 5805–5863.
[9] A. Bogaerts, G. Centi, Front. Energy Res. 8 (2020) 111.
[10] R. Vertongen, A. Bogaerts, J. CO_2 Util. 72 (2023) 102510–102531.
[11] M. Ramakers, G. Trenchev, S. Heijkers, W. Wang, A. Bogaerts, ChemSusChem 10 (2017) 2642–2652.
[12] A. Hecimovic, F.A. D'Isa, E. Carbone, U. Fantz, J. CO_2 Util. 57 (2022) 101883.
[13] E.R. Mercer, S. Van Alphen, C.F.A.M. van Deursen, T.W.H. Righart, W.A. Bongers, R. Snyders, A. Bogaerts, M.C.M. van de Sanden, F.J.J. Peeters, Fuel 334 (2023) 127565.
[14] A. Hecimovic, C.K. Kiefer, A. Meindl, R. Antunes, U. Fantz, J. CO_2 Util. 71 (2023) 102473–102481.
[15] R. Antunes, K. Wiegers, A. Hecimovic, C.K. Kiefer, S. Buchberger, A. Meindl, T. Schiestel, A. Schulz, M. Walker, U. Fantz, ACS Sus. Chem. Eng. 11 (2023) 15984–15993.
[16] R. García, C. Pizarro, A.G. Lavín, J.L. Bueno, Fuel 195 (2017) 182–189.
[17] S. Ullah, S.S.A. Shah, M. Altaf, I. Hossain, M.E. El Sayed, M. Kallel, Z.M. El-Bahy, A.U. Rehman, T. Najam, M.A. Nazir, J. Anal. Appl. Pyrolysis 179 (2024) 106480–106510.
[18] F. Girard-Sahun, O. Biondo, G. Trenchev, G. van Rooij, A. Bogaerts, Chem. Eng. J. 442 (2022) 136268–136284.
[19] H.S. Uhm, H.S. Kwak, Y.C. Hong, Environ. Pollut. 211 (2016) 191–197.
[20] P. Liu, X.S. Liu, J. Shen, Y.X. Yin, T. Yang, Q. Huang, D. Auerbach, A.W. Kleiyn, Plasma Sci. Technol. 21 (2019) 044003.
[21] Z.K. Li, T. Yang, S.J. Yuan, Y.X. Yin, E.J. Devid, Q. Huang, D. Auerbach, A.W. Kleyn, J. Energy Chem. 45 (2020) 128–134.
[22] J.Y. Huang, H. Zhang, Q.H. Tan, L. Li, R.Y. Xu, Z.M. Xu, X.D. Li, J. CO2 Util. 45 (2021) 101432.
[23] H. Zhang, Q.H. Tan, Q.X. Huang, K.Y. Wang, X. Tu, X.T. Zhao, C.F. Wu, J.H. Yan, X. D. Li, ACS Sustain. Chem. Eng. 10 (2022) 7712–7725.
[24] Y. Wu, S.Z. Li, Y.L. Niu, H.J. Yan, D.Z. Yang, J.L. Zhang, J. Phys. d: Appl. Phys. 56 (2023) 065201–065214.
[25] T. Nunnally, K. Gutsol, A. Rabinovich, A. Fridman, A. Gutsol, A. Kemoun, J. Phys. D: Appl. Phys. 44 (2011) 274009–274017.
[26] L. Fulcheri, F. Fabry, S. Takali, V. Rohani, Plasma Chem. Plasma Process. 35 (2015) 565–585.
[27] S.A. Wutzke, E. Pfender, E.R.G. Eckert, AIAA J. 5 (1967) 707–708.
[28] I. Tsonev, C. O'Modhrain, A. Bogaerts, Y. Gorbanev, ACS Sus. Chem. Eng. 11 (2023) 1888–1897.
[29] B. Wanten, R. Vertongen, R. De Meyer, A. Bogaerts, J. Ener. Chem. 86 (2023) 180–196.
[30] C. O'Modhrain, G. Trenchev, Y. Gorbanev, A. Bogaerts, ACS Eng. Au 4 (2024) 333–344.
[31] F.A. D'Isa, E.A.D. Carbone, A. Hecimovic, U. Fantz, Plasma Sources Sci. Technol. 29 (2020) 105009.
[32] S. Lee, J. John, G. Park, J.G. Kim, Appl. Compos. Mater. 28 (2021) 529–557.